

Part I
Single-Particle Imaging and Tracking

1

Three-Dimensional Particle Tracking in a Laser Scanning Fluorescence Microscope

Valeria Levi and Enrico Gratton

1.1 Introduction

In recent years, single-particle and single-molecule techniques have each become essential tools in the fields of biophysics and cell biology [1]. One of the main reasons for the strong impact of these techniques is that they provide crucial information that is averaged out in traditional ensemble methods. Among these new techniques, single-particle tracking (SPT) has constituted a remarkable new tool for the study of dynamics in biological processes.

Today, several fluorescence microscopy techniques have been developed to measure the motion of molecules, the two most widely used being fluorescence recovery after photobleaching (FRAP), which was developed during the 1970s by Axelrod *et al.* [2], and fluorescence fluctuation spectroscopy (FFS), which was established during the same decade by Magde *et al.* [3]. Some of the most important characteristics of these techniques are represented schematically in Figure 1.1. While FRAP averages, in time and space, the behavior of a large ensemble of molecules, FCS averages the behavior of a small number of molecules within the observation volume. In both cases, the mobility properties determined in these experiments correspond to the average behavior of the observed molecules. Such averaging may, however, be problematic. For example, one problem may occur in the complex environment of the cell, where particles can interact with multiple targets and result in populations with different mobility properties. Moreover, the dynamics of each population may change in time and/or space. In such cases, both FRAP and FCS will provide only limited dynamical information.

Although SPT was first applied in biophysics during the 1980s and 1990s [16–19], the number of applications of these techniques has since grown significantly, based mainly on advances in microscopy and labeling techniques which have led to significant improvements in the accuracy and speed of these methods. Such advances have also presented the possibility to study more complex processes, with better spatial and temporal resolution.

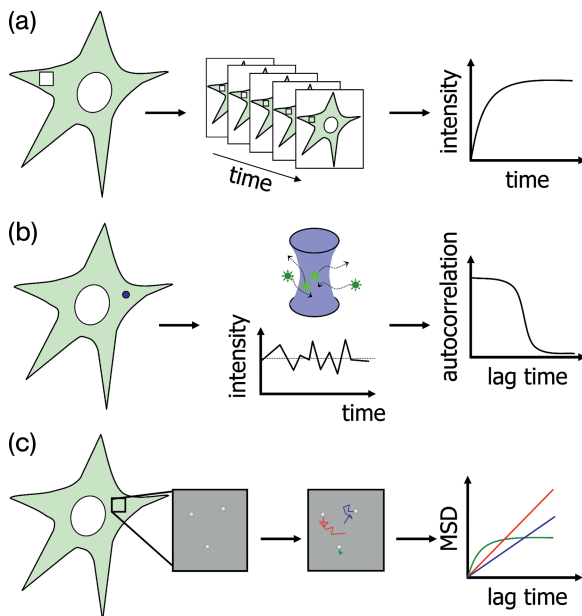


Figure 1.1 Studying dynamics with fluorescence microscopy. (a) Fluorescence recovery after photobleaching (FRAP) (for a review, see Ref. [4]) involves the selective photobleaching of fluorescent molecules in a given region (shown as a white square) of a sample with a high-intensity laser, followed by measurement of the recovery of fluorescence intensity in the bleached region as a function of time. The recovery kinetics depend on the speed at which the fluorescent particles move from other regions of the sample to the photobleached area, and provides information regarding the mobility of the labeled molecules; (b) Fluorescence fluctuation spectroscopy (FCS) and related techniques [5–7] measure fluctuations in fluorescence intensity in the femtoliter observation volume (blue) obtained in a confocal or two-photon microscope. These fluctuations are due to fluorescent molecules moving in and out of the observation

volume (green stars), and their quantitative analysis through calculation of the autocorrelation function provides information regarding the average residence time, and therefore the mobility of the labeled molecules in that volume; (c) Single-particle tracking (SPT) determines the trajectories of single particles within the sample. These trajectories are analyzed to extract quantitative information regarding the motion mechanism of the particles [8]. The most common approach to analyze single-particle trajectories is to calculate the mean-square-displacement (MSD) as a function of the lag time. This parameter indicates how far a particle has traveled, and its dependence with τ is related to the motion properties of the particle. Consequently, a possible mechanism of motion can be obtained by comparing the experimental MSD plot with predictions from theoretical motion models [8–15].

These fluorescence microscopy techniques were developed to follow the position of individual particles in time. Provided that the spatial and temporal resolution of the method is adequate, these trajectories can be analyzed statistically to extract quantitative information regarding the mechanism involved in the motion of the particle (for recent reviews, see Refs [8, 20]). Since the properties of

the particles are not averaged (as in bulk measurements), SPT represents an appealing technique to achieve the ultimate goal of understanding dynamics within cells.

In this chapter, we briefly describe the techniques that are used most often for tracking particles, and focus on recent advances in microscopy that have led to improvements in these methods. We discuss the different strategies employed to obtain information with regards to the axial position of the particle in image-based tracking approaches, and describe in detail a routine designed to achieve three-dimensional (3-D) tracking, using laser scanning microscopy. Finally, applications of the technique to the study of chromatin dynamics in interphase cells are demonstrated, the aim being to highlight possible applications for this new tracking procedure.

1.2 Image-Based Single-Particle Tracking Methods

The methods used most often to track fluorescent particles are based on recording images of the sample in a widefield or confocal fluorescence microscope as a function of time, and then locating the particle of interest in every recorded frame of the stack by using a specific algorithm (Figure 1.2).

In an optical microscope, a point-like particle forms a diffraction-limited image of width approximately equal to $\lambda/(2NA)$, where λ is the wavelength of the light and NA is the numerical aperture of the objective. This diffraction limit implies that the image of the particle would have a diameter of ~ 200 nm for visible light. Thus, if particles are close to each other within this diffraction limit, it is not possible to determine their individual positions.

When the distances among particles exceed this limit, however, the position of each particle will correspond to the center of the intensity distribution of its image. In such cases, this position can be determined with high precision by using an algorithm that identifies the center of the distribution [21, 22]. For example, Yildiz *et al.* located molecular motors that had been labeled with single fluorophores, with an error of 1.5 nm, by fitting a Gaussian function to the intensity distribution of the fluorophore image [23, 24].

Recently, the present authors have designed a pattern recognition algorithm with 2 nm accuracy and 10 ms temporal resolution, which does not require the assumption of an intensity distribution function for the particle as it uses the particle's own intensity profile [25]. This approach improves the precision with respect to other techniques when tracking particles of finite size. Moreover, the algorithm makes it possible to correct for an inhomogeneous background, which is ideal for tracking experiments in living cells.

Importantly, these approaches only provide information regarding the two-dimensional (2-D) motion of particles at the focal plane. Those particles that move away from this plane will change their intensity profile until they completely disappear from the image. Thus, these techniques have been mainly used to study

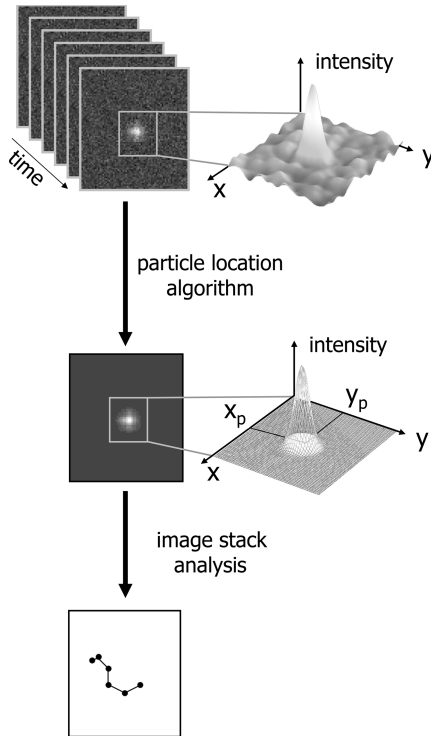


Figure 1.2 Image-based methods for single-particle tracking. The image of a fluorescent point-like particle observed through a fluorescence microscope shows an intensity distribution, the center of which corresponds to the position of the particle. This position (x_p, y_p) can be recovered by using a deconvolution algorithm which, for

example, fits the experimental intensity of the image with a known distribution function allowing determination of the center of the image. This routine is repeated in every image of an image-stack acquired as a function of time to calculate the particle trajectory.

processes that occur in two dimensions, such as the diffusion of membrane components [26–28] and their transport along cytoskeleton filaments positioned within the focal plane [16, 23].

When using the SPT routine, it is important to analyze the factors that determine the precision of the particle position calculation. Thompson *et al.* [29] studied the theoretical sources of noise in the determination of particle position when fitting the image of a single fluorophore with a Gaussian distribution function and obtained the following expression:

$$\langle(\Delta x)^2\rangle = \frac{s^2}{N} + \frac{a^2}{12N} + \frac{8\pi s^4 b^2}{a^2 N^2} \quad (1.1)$$

where Δx is the error in the particle position, s is the standard deviation of the point spread function (PSF), a is the pixel size, N is the number of photons col-

lected, and b is the background noise, which includes fluorescence coming from the background and the noise of the detector.

The first term arises from the photon noise, which results from the fact that photon emission is a random process that follows a Poissonian distribution. Thus, this error represents the fluctuations in the number of photons collected in a given temporal window. The second term is the pixelation noise, and is due to the finite size of the pixels. This noise arises from the uncertainty as to where the photon arrived in the pixel, and thus increases the apparent size of the image spot. Thompson *et al.* [29] demonstrated that, in practice, the pixel size should be in the region of the standard deviation of the PSF. The final term is related to the background noise, and represents the error introduced on the position determination by photons coming from sources other than the particle. Common sources of background noise include readout error, dark current noise, and autofluorescence of the sample.

1.3

Advanced Fluorescence Microscopy Techniques for Single-Particle Tracking

One of the main problems encountered with SPT approaches based on standard epifluorescence microscopy is that excitation occurs throughout the entire depth of the specimen. Consequently, fluorescence derived from regions far away from the focus will increase the background intensity, and in turn decrease the effective signal-to-noise ratio (SNR) of single particles at the focal plane. These out-of-focus regions are also unnecessarily photobleached and photodamaged. For single-particle tracking experiments, these factors will lead to reductions not only in the accuracy of the tracking but also in the effective duration of the tracking experiments.

Confocal microscopy (for a review, see Ref. [30]) constituted an improvement in widefield approaches due to its ability to reject out-of-focus light. In most commonly used confocal microscopes set-ups, the sample is excited by epillumination with a laser, while the objective collects the fluorescence emitted at the diffraction-limited volume. The emission passes through the dichroic mirror and an emission filter, is focused at an aligned confocal aperture or pinhole exactly in the primary image plane of the objective, and is then detected with a photomultiplier tube or avalanche photodiode detectors. Fluorescent light from above and below the primary image plane come to a focus elsewhere, and so must be defocused at the confocal aperture. Consequently, they will not reach the detector, which in turn will thus eliminate the blurring of images caused by out-of-focus light, as is observed in standard epifluorescence microscopes.

This simple set-up allows detection of fluorescence from a single point in the sample. To reconstruct an image, it is necessary to move either the sample or the excitation laser in such a way that the laser can scan a given region of interest. Generally, the excitation laser is raster-scanned by using two galvanometer scanning mirrors. In this conventional confocal set-up, the image acquisition fre-

quency is normally less than 10 frames per second, because not only must the laser scan the sample, but it is also necessary to integrate the intensity signal during at least $10\mu\text{s}$ per pixel. By contrast, the image acquisition time in widefield set-ups normally ranges from 1 to 30 ms [31–35], but may be as short as $25\mu\text{s}$ [27]. Thus, conventional confocal microscopy is useful only for single-particle tracking studies of processes with very slow dynamics.

Modifications of this original set-up have been carried out for the observation of fast dynamics. In the *spinning-disk confocal microscope*, a rapidly rotating disk with an array of pinholes is used to generate an array of beams that are focused on the sample. The pinholes on the disk are arranged in a pattern that allows every location of an image to be covered when the disk is rotated. The fluorescence is collected through the same set of pinholes, and focused in a charge-coupled device (CCD) camera. Instead of scanning one point at a time, a spinning disk confocal microscope can measure the intensity of a thousand points of the sample simultaneously; consequently, the image acquisition frequency can be increased to approximately 300 frames per second (for a review, see Ref. [36]). Recent examples of the use of spinning disk confocal microscopy include the tracking of cytoplasmic and nuclear HIV-1 complexes [37], and the monitoring of mRNA transport [38].

Total internal reflection fluorescence (TIRF) microscopy represents an interesting alternative to standard epifluorescence microscopy for SPT experiments (for recent reviews, see Refs [39, 40]). In a TIRF microscope, excitation is achieved with an evanescent field generated by total reflection of the excitation laser. As this evanescent field decays exponentially with the distance normal to the surface, excitation of the fluorophores can only occur within 100 nm of the specimen surface. This presents a significant minimal reduction in out-of-focus background with respect to widefield and confocal approaches. Also, as no excitation occurs in regions far from the thin evanescent field, both photodamage and photobleaching are significantly lower than in standard fluorescence microscopy. Because of its strong dependence with the distance, SPT-TIRF microscopy has been used successfully to study the dynamics of biomolecules nearby, or inserted into, biological membranes [41], and the processes occurring at the coverslip surface [23, 42].

During the past decade, super-resolution, far-field microscopy techniques have successfully overcome the diffraction limit [43–50]. For example, stimulated emission depletion (STED) microscopy generates fluorescent focal spots that are smaller than what might be predicted according to the diffraction limit. In this type of microscope, the focal spot of an excitation laser is overlapped with doughnut-shaped spot of another laser of lower photon energy that quenches excited molecules in the excitation spot periphery by stimulated emission. As a result of the stimulated emission, the excitation volume is effectively reduced in size, such that resolution down to 20 nm can be achieved [43]. Imaging with these techniques usually takes longer than with conventional widefield techniques; consequently they are mainly applied to the study of fixed specimens [51–54]. However, in a recent study reported by the group of Hell, the STED-imaging of synaptic vesicles was demonstrated at video-rate in living neurons [55]. Clearly, a growing number

of applications of these exciting new techniques for SPT studies in living cells is to be expected in future.

1.4

Two-Photon Excitation Microscopy

Although two-photon absorption was originally predicted by Maria Göppert-Mayer in 1931, this important principle could not actually be demonstrated until the development of high-intensity lasers [56]. In fact, several more years were to pass until two-photon excitation was first applied to laser scanning microscopy [57], some excellent reviews of which are available [58–61].

Two-photon excitation (TPE) is a nonlinear process that involves the almost simultaneous absorption of two photons ($\sim 10^{-16}$ s) that, in the simplest case, will have half of the energy required for transition to the excited state (Figure 1.3a). Two-photon excitation is typically achieved with near-infrared (NIR) excitation sources, because most common dyes used in fluorescence microscopy absorb in the ultraviolet (UV) or visible spectral region.

As the molecular cross-sections for two-photon absorption are very small, ($\sim 10^{-56}$ cm⁴ s per photon; [59]), high photon fluxes are required to achieve significant levels of fluorophore excitation. For this reason, TPE requires high-power continuous-wave lasers or femtosecond-pulse lasers that provide pulses of high intensity during brief periods of time, but have a low average excitation power, which limits the heating of the sample.

The TPE probability is proportional to the square of the laser intensity, which implies that TPE will only occur at the focus of the laser, where the photon flux is highest [60]. Figure 1.3b shows the emission volumes obtained in a solution of a fluorescent probe under two-photon or one-photon excitation. While two-photon excitation occurs only in the femtoliter volume in which the laser was focused, one-photon excitation is also observed in out-of-focus regions.

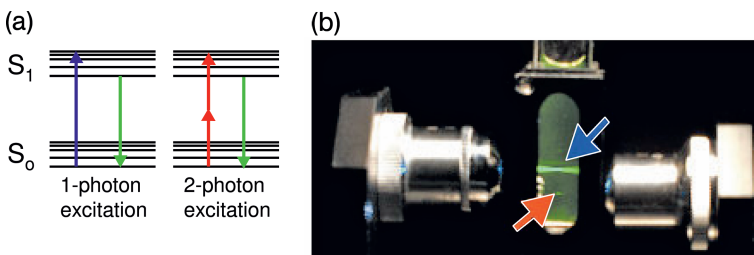


Figure 1.3 Two-photon excitation microscopy. (a) Energy diagrams showing the electronic transitions occurring during one-photon (blue) and two-photon (red) excitation; (b) Emission volumes obtained in a fluorescein solution excited under one-photon (blue arrow) and two-photon (red arrow) conditions. The numerical apertures of the objectives used in this experiment were the same. Reproduced with permission from Ref. [60]; © 2000, Annual Reviews (www.annualreviews.org).

This intrinsic, optical 3-D sectioning capability is the most appealing characteristic of TPE for fluorescence microscopy, as it is possible to perform 3-D imaging as in a confocal microscope, without the need for a confocal pinhole. Moreover, as most biological samples do not absorb significantly in the IR range, the out-of-focus regions will not contribute to the background and so will not be photodamaged.

The background fluorescence in two-photon microscopy is also reduced by the fact that the excitation is significantly red-shifted with respect to the emission. Thus, it is easier to separate emission light from the excitation beam than in a one-photon experiment, where they may be spectrally close together. Another advantage of two-photon microscopy is that it can be used for imaging thick specimens; this is because the NIR light employed for the excitation is less scattered and absorbed than the UV or visible excitation light required for the excitation of common fluorophores in one-photon microscopy.

The main drawback of TPE fluorescence microscopy is that photobleaching within the focal volume, with laser power levels typically used in biological imaging, is usually much more extensive than would be expected for one-photon excitation, and may be attributable to higher-order resonance absorption [59].

1.5

3-D Tracking in Image-Based SPT Approaches

The initial methods developed for 3-D tracking utilized confocal or two-photon microscopy to achieve a z-sectioning of the specimen, and consisted of collecting z-stacks as a function of time. The resultant stacks of images were analyzed using a deconvolution algorithm to locate the particle of interest with high precision [37, 62]. However, these methods required the sample to be scanned several times, which made the tracking very slow for most applications.

One interesting possibility of obtaining the z-position of a particle simply by analyzing the 2-D images was proposed by Speidel *et al.* [63]. This group made use of the fact that the image of a point-like particle changes when it is defocused. The spot diameter increases and, for large z-displacements from the focus, ring intensity patterns are formed. Thus, the distance of the object to the imaging focal plane is encoded in the intensity pattern. Speidel's group observed that the radius of the outermost ring was linearly related to the actual z-position, and used this relation to calculate the axial position of the particle (Figure 1.4). This method can be used to follow particles moving within a range of 3 μm from the focal plane, with an accuracy of approximately 1 nm and a time resolution of about 100 ms. However, the accuracy in the radial position was seen to decrease with the distance from the focal plane, as the intensity of the off-focus images was spread over a higher number of pixels.

In order to improve the radial position accuracy, different groups have used multifocal imaging methods in which two or more focal planes about the

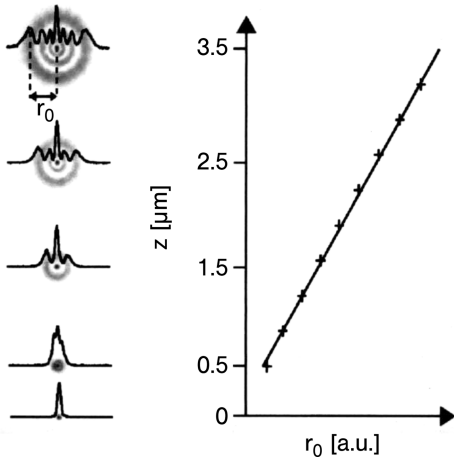


Figure 1.4 Three-dimensional defocusing-based SPT techniques. Images of a fluorescent bead in an agarose gel at different z -distances from the focal plane (left). The radius r_0 of the outermost ring in the images scaled linearly with z (right). Reproduced with permission from Ref. [63]; © Optical Society of America.

selected particles of interest were recorded, either with different cameras or on separate halves of a single CCD camera [64, 65]. The radial and axial positions of the particle which were obtained by analyzing the focused and defocused planes, respectively, could be determined with 2–5 nm accuracy and 2–50 ms time resolution [65].

A similar defocusing-based approach was previously followed by Kao *et al.* [66], who introduced a cylindrical lens into the detection optical path of a widefield fluorescence microscope, the aim being to generate axial astigmatism in the collected image. As a result, the images of point-like or spherical fluorescent particles were circular in focus but ellipsoidal above and below the focus, with the major axis of the ellipsoid shifted by 90° in going through the focus. Thus, the absolute z -position of the particle can be determined from the image shape and orientation. Holtzer *et al.* [67] further improved this method to track single quantum dots (QDs) in cells, and attained 6 and 30 nm accuracy in the lateral and axial position of the dots, respectively. Hence, this tracking routine appears to function for particles within $1\ \mu\text{m}$ of the focal plane.

Recently, Saffarian *et al.* [68] established a new image-based 3-D tracking method that combines widefield and TIRF microscopy, based on the earlier studies of Sarkar *et al.* [69]. These authors determined, experimentally, the distance-dependence of the evanescent field and related the emitted photons of a single particle with its position in this field, achieving an axial accuracy of 10 nm.

1.6

3-D Tracking in Laser Scanning Microscopes

Previously, it was noted that image-based 2-D tracking methods for confocal and TPE microscopy had very low temporal resolution, mainly because it was necessary to scan the laser through the region of interest. Moreover, 3-D tracking required the acquisition of a z-stack of images for each tracking time, which made the procedure even slower.

A completely different approach for tracking particles in three dimensions, using a TPE microscope, was introduced by the present authors' group [70–72], based on the earlier studies of Enderlein [73].

In this approach, the laser is scanned in circles of diameter equal to the PSF radial waist surrounding the particle of interest. The fluorescence intensity is integrated at given points of these orbits as the laser moves around the particle. The scanner performs a given number of orbits, n , which are averaged to improve the SNR. When the laser has finished these orbits, a z -nanopositioner moves the objective to a different z -plane, where the orbits are repeated. The two z -planes are separated from each other by the z -waist of the PSF. The particle position is recovered from the intensity data obtained in a cycle of scanning (e.g., n orbits in the two different z -planes), as described below.

Kis-Petikova and Gratton [70] and Berland *et al.* [74] have demonstrated that the fluorescence intensity (F) during scanning is a periodic function of time (t):

$$F(t) = \frac{2F_0/\pi}{1 + \frac{\lambda^2(z_p - z_s(t))^2}{w_0^4\pi^2}} \exp \left[-\frac{2[(x_p - x_s(t))^2 + (y_p - y_s(t))^2]}{w_0^2 + \frac{\lambda^2(z_p - z_s(t))^2}{w_0^2\pi^2}} \right] + B \quad (1.2)$$

where w_0 is the beam waist, λ is the wavelength, B is the background intensity, and F_0 is a constant related to the peak fluorescence intensity. The subscripts p and s refer to the particle and the scanner coordinates, respectively. According to the description above, the scanner coordinates vary as a function of time as follows:

$$\begin{aligned} x_s(t) &= r_{xy} \cos(2\pi f_{\text{orbit}}t) \\ y_s(t) &= r_{xy} \sin(2\pi f_{\text{orbit}}t) \\ z_s(t) &= \begin{cases} r_z & 0 < \frac{f_{\text{orbit}}t}{n} < 1, 2 < \frac{f_{\text{orbit}}t}{n} < 3, \dots \\ -r_z & 1 < \frac{f_{\text{orbit}}t}{n} < 2, 3 < \frac{f_{\text{orbit}}t}{n} < 4, \dots \end{cases} \end{aligned} \quad (1.3)$$

where r_{xy} is the xy -circular orbit radius, r_z is half the amplitude of the z -square wave, f_{orbit} is the frequency of the circular orbit, and n is the number of circular orbits made before changing the z position.

According to these equations, the absolute position of the particle (x_p , y_p , z_p) is encoded in the fluorescence intensity registered during the tracking cycle. Figure 1.5a shows intensity profiles expected for particles situated at different positions

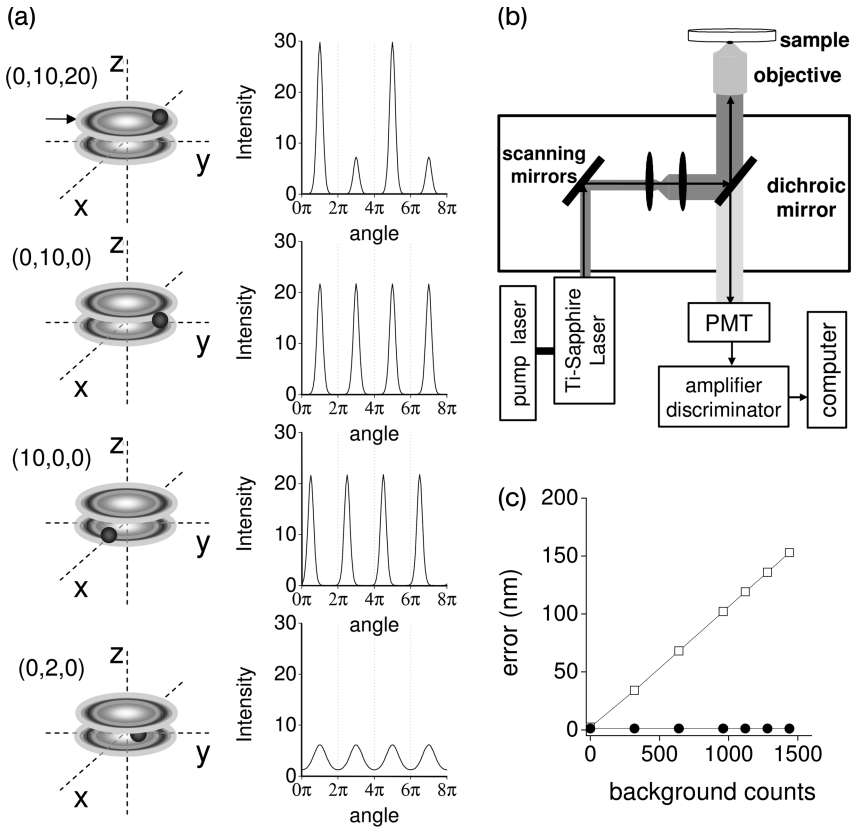


Figure 1.5 Tracking in a two-photon excitation (TPE) microscope. (a) The intensity profile determined along two cycles of the tracking routine is represented as function of the angle of rotation of the laser, for different relative positions of the particle with respect to the center of scanning (right panels). In the examples, each cycle of the tracking routine consisted in two orbits, each one at a different z-plane. The left panels show diagrams of the relative position of the particle (dark circle) with respect to the center of scanning. The laser orbits are represented as ovals. The arrow shows the starting point of the tracking cycle. The right panel shows the measured fluorescence intensity. (b) Schematic of the TPE microscope used for single-particle tracking experiments. PMT = photomultiplier tube. (c) The error for the orbiting-based routine

(filled circles) was calculated as the standard deviation of the radial position recovered for a fixed particle after 1000 cycles of tracking in two dimensions. The background counts are the average number of counts measured during each cycle of the tracking routine in the absence of the particle. The background noise was assumed to have a Poisson distribution. For comparison, the error from the Gaussian-fitting routine (open squares) calculated from Equation 1.1 is shown. In both cases, it was assumed that the total number of photons detected from the particle was 12000, either during one cycle of the circular-scanning routine or in one frame of the Gaussian-fitting routine. The pixel size and waist of the point spread function were 250 nm. (a) and (c) reproduced from Ref. [20] with permission from Springer Science+Business Media.

relative to the scanning center. Kis-Petikova and Gratton [70] demonstrated that the particle coordinates could be calculated from the phase and modulation obtained by fast Fourier transform (FFT) of the intensity signal measured during a tracking cycle. This approach is much faster than fitting Equation 1.2 to the intensity trace, and can be achieved “on-the-fly,” which is essential for this tracking routine.

The procedure, as described thus far, does not allow tracking of a moving particle as the intensity will drop to zero when the particle moves away from the center of the scan. In order to continuously track a particle, its position must be determined on-the-fly (as described above); then, using a feedback loop, the center of scanning must be moved to the new position of the particle where a new cycle of the tracking routine starts. In other words, during the tracking routine, the scanner follows the particle by changing its position to that calculated for the particle in the previous cycle. In an ideal tracking experiment, the scanner is always on top of the particle, such that the positions of the scanner and the calculated position for the particle are identical.

By using this procedure it was possible to locate single particles with a precision of 20 nm [71] in approximately 16 ms when tracking in two dimensions, and in 32 ms when tracking in three dimensions. As the laser follows the particle in three dimensions, the x , y and z ranges in which the tracking routine works are only limited by the working range of the (x,y) scanning mirrors (see below) and the working distance of the objective, respectively.

A method related to the above-described orbiting method has been proposed by Lessard *et al.* [75]. Here, the experimental set-up is very similar to a confocal microscope, in that a one-photon excitation laser is focused on the sample, while fluorescence emitting from a particle located within the excitation volume is collected by four optical fibers. These fibers act as confocal pinholes, with each one coupled to an avalanche photodiode detector. The fiber faces are arranged in pairs such that their projection back into the sample space forms a tetrahedron. The 3-D position of the particle is recovered in 5 ms by analyzing the different signals collected by the detectors. Each pair of fibers is aligned to provide the position of the particle in the x and y axes; the two pairs of fibers are then offset along the optical axis, which enables location of the particle in the z direction. Based on the results of simulations, these authors reported an error on the particle position determination of approximately 200 nm. Tracking is achieved by using a feedback algorithm similar to that described before; the position of the particle is determined after a cycle of tracking, and the sample stage is then moved so as to bring the target closer to the center of the laser focus.

1.7

Instrumentation

In the two-photon microscope set-up used for the 3-D orbital tracking routine (see Figure 1.5b), a mode-locked titanium–sapphire laser is used as the excitation source. These lasers are ideal for two-photon microscopy because they provide

femtosecond pulses with a repetition rate of ~ 100 MHz, and can be tuned in the range of 700–1000 nm so as to cover the excitation of common fluorescent probes, including most of the variants of fluorescent proteins. The laser is then directed into the microscope by two galvomotor-driven scanning mirrors controlled by the voltage generated from a computer card. When the mirrors are synchronized to move with sine waves shifted by 90° relative to one another, the laser beam moves in a circular path, with a radius determined by the amplitude of the sine waves. The position of the center of scanning is given by the offset values of the sine waves.

The laser light is reflected in a low-pass dichroic mirror and focused onto the sample by the objective. Fluorescence emission is collected by the objective and passed through the dichroic mirror and a short-pass filter to eliminate any reflected excitation light. The emission beam then exits the microscope to the photomultiplier detector with single-photon counting capability, and the photons are counted using a data acquisition card.

To enable changes of the focal plane, a piezoelectric z -nanopositioner equipped with a linear voltage differential transformer feedback sensor, and operated in a closed-loop configuration, is placed below the objective. During each cycle of the tracking routine the computer card generates a square-wave voltage which drives the motion of the z -nanopositioner between two z planes that are separated by a distance given by the amplitude of the square wave. The position of the center of z -scanning is given by the DC offset.

1.8

Background Noise

It is predicted by Equation 1.1 that the position of a particle obtained by Gaussian fitting depends sensitively on the intensity of the background. In Figure 1.5c, it is shown that the determination accuracy of the particle position decreases abruptly upon adding a background representing a small percentage of the total counts. Thus, extreme care must be taken when using this method, and its application should be restricted to cases in which the brightness of the particle is high. In contrast, the precision of particle position determination when using a tracking routine based on circular scanning is approximately constant with the background intensity in a wide range, due to the fact that the FFT of the intensity signal is not affected by a locally homogeneous background noise. Thus, the orbiting method described here has a major advantage with respect to image-based approaches when dealing with samples that have high background levels.

1.9

Simultaneous Two-Particle Tracking

The main disadvantage of the orbiting method is that it allows the tracking of only one particle at a time, although the routine may be modified to recover the position

of two (or more) different particles successively. The tracking routine starts on top of one of the particles and, after one tracking cycle, the laser is moved to the position of the second particle to collect another cycle. When this second cycle is finished, the center of scanning is moved back to the position determined in the previous cycle for the first particle, and so on. In this way the positions of the particles are recovered alternately. This method does not require the particles to be at the same *z*-plane; rather, they can be followed even if they move several microns away from each other in the axial direction. The only requirement is that the particle is still in the vicinity where it was last seen when the algorithm returns. As the positions of the particles are recovered successively, the overall time resolution is cut in half; in other words, when tracking two particles, the time taken to obtain each particle position will be twice that required for the single-particle tracking mode.

The two-particle tracking option represents an interesting choice when conducting SPT tracking experiments in living cells, because the cells may migrate during the experiment and complicate any interpretation of the results. In some cases this problem can be corrected by using an internal reference—that is, a second particle located close to the studied particle. Then, if both particles are moving according to the same mechanism, the analysis of the temporal evolution of the distance between them will provide information regarding their motion [76]. Moreover, if one of the particles can be considered fixed, then the distance between them will provide information regarding the intrinsic motion of the particle [77].

1.10

Application: Chromatin Dynamics in Interphase Cells

The organization of chromatin in interphase nuclei has been the subject of much debate over the past decade [78], with several reports suggesting (e.g., [79–82]) that the chromosomes occupy well-defined volumes within the nucleus, termed “chromosomes territories.” In fact, a significant amount of evidence has accumulated recently pointing towards a model in which a specific local reorganization of regions of these territories occurs in order to activate transcription [81, 83–86]. These antecedents show that the spatial organization of chromatin is intimately related to gene expression. However, the most important – and as yet unanswered – questions relate to how the chromatin organization is achieved, and how specific regions change their position within the nucleus.

A major breakthrough in this field was made with the development of a method whereby specific DNA sequences in live cells could be labeled by the insertion of lac operator repeats at specific chromosome locations. This locus could then be detected through binding of the lac repressor protein fused to green fluorescent protein (GFP) and engineered to contain a nuclear localization signal [87, 88]. The fluorescently labeled sequence could be identified as a bright dot in the nucleus, which itself would be dimly fluorescent due to the unbound EGFP-Lac repressor

(a)

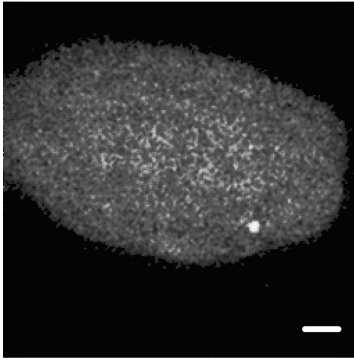
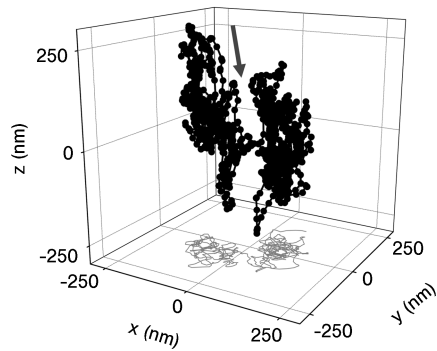


Figure 1.6 Studying the dynamics of chromatin in living cells by SPT. (a) A TPE fluorescence image of a representative cell containing an eGFP-labeled chromatin sequence. Scale bar = $2\mu\text{m}$ Reproduced with permission from Ref. [72]; © 2005,

(b)



Biophysical Society. (b) The trajectory was collected with a time resolution of 32 ms. To facilitate the visualization of a region of curvilinear motion (arrow), the (x,y) projection of the trajectory is also shown (gray).

(Figure 1.6a). The motion of this bright dot could then be followed, and the recovered trajectory analyzed to obtain information concerning the mechanism by which the tagged sequence had moved.

By using image-based tracking approaches, several groups have shown that, during interphase, the GFP-tagged chromatin loci undergo Brownian motion which is limited to a subregion of the nucleus [76, 89, 90]. This motion seemed to be more complex than constrained, passive diffusion, however. For example, Rosa *et al.* [91] showed that two chromosomal sites which exhibited a preferential association with the nuclear membrane were confined to regions of different size, with the site having higher levels of transcription exploring larger regions. Tumbar and Belmont [92] also showed that a specific DNA region in Chinese hamster ovary (CHO) cells could change its position, from the nucleus periphery to the center, in response to VP16 transcriptional activator.

One important factor that limits the temporal resolution and observation time window in studies of chromatin dynamics is that the motion of the labeled sequence is highly sensitive to photodamage [93, 94]. For example, Chuang *et al.* [94] showed that the motion of a tagged chromatin sequence was significantly altered after taking as few as 10 images when using a mercury lamp as an excitation source, under regular imaging conditions.

Subsequently, the dynamics of enhanced GFP (eGFP)-tagged chromatin sequences in interphase cells were reinspected by using the two-photon microscopy tracking technique described above [72]. As noted previously, TPE normally causes less out-of-focus photobleaching and photodamage than does one-photon excitation. In addition, the excitation laser moves within a very small volume of the cell during the tracking routine, and consequently does not introduce

any damage in regions far from the tagged sequence. For these measurements, a typical spatial resolution of 20 nm was employed at a temporal resolution of 30 ms.

The trajectories obtained for the eGFP-tagged sequence showed long periods of confinement in regions where the size was similar to the 30 nm fiber of chromatin. This probably reflected local, thermal fluctuations, interspersed by short periods in which the sequence moved approximately 150 nm and followed a curvilinear path. An example of one such trajectory, obtained by tracking the sequence motion in three dimensions, is shown in Figure 1.6b.

The presence of these jumps in position was intriguing, since (to the present authors' knowledge) they had not been observed previously in any study relating to chromatin motion. Moreover, as the jumps occurred within a time range of 0.3–2 s, they could not be observed using a tracking method with a low temporal resolution. The characteristic jump distance of 150 nm was also similar to the spatial resolution of previously used methods.

The possibility of the jumps being due to motion of the nucleus was also eliminated by the use of a second cell line that presented multiple lac operator-repeats insertions, and also expressed the EGFP-lac repressor protein. Each of the insertions was visualized by fluorescence microscopy as a bright dot that was separated from neighboring dots by less than 1–2 μm . Whilst the trajectories of these labeled DNA sequences also presented jumps, they occurred independently from each other; this indicated that the jumps reflected local, short-distance motions of the chromatin sequence.

Consequently, a set of new, statistical tools was designed to obtain insight into the mechanism underlying the motion of the sequence during jumps. These analyses were complemented by experiments which tested the hypothesis derived from the statistical analysis. The statistical analyses were designed to compare the motion of the sequence during jumps with the predictions obtained by considering only a passive diffusion process. Ultimately, the results of all analyses indicated that, on average, the sequence moved fourfold faster than during the periods between jumps, and followed paths that were more rectilinear than might be predicted for random diffusion motion. Overall, these data suggested that an active process was responsible for transport of the sequence during short periods of time. Moreover, the hypothesis was supported by experiments which showed that no jumps occurred in the trajectories following ATP depletion. It appeared, therefore, that the jumps most likely reflected energy-dependent chromatin movements.

1.11

Conclusions

In recent years, SPT techniques have provided unique information with regards to the dynamics of processes in a wide variety of systems, most notably in the field

of cell biology. The relevance of these new techniques is reflected by the fact that the number of reports in which SPT has been applied has grown exponentially with time.

The main reasons for such growth has been the development of new microscopy techniques and their application to SPT studies, as well as improvements in the technology required (e.g., CCD cameras) and the development of new tracking routines. Together, these contributions have led to significant advances in both the speed and spatial resolution of SPT.

Over the past few years, much effort has been expended in the design of SPT techniques capable of recovering the trajectories of particles in three dimensions. In this chapter, we have described several methods designed to track in three dimensions, and also introduced a new technique which is based on a two-photon microscopy set-up and offers several advantages with respect to the classical, image-based methods. The new method has high spatial and temporal resolution and, in contrast to image-based approaches, is able to follow the particle even when it moves several microns from its original position. The level of photodamage to the sample, which is introduced during tracking with the orbiting method, is substantially low as the laser is consistently on top of the tracked particle such that the remainder of the sample is not exposed to the excitation light. The tracking is also relatively insensitive to the background noise, which makes it suitable for applications that involve high levels of background intensity, for example, in living cells.

One important characteristic of the orbiting tracking method is that the trajectory is measured on-the-fly, in contrast to other approaches where the trajectory of the particle is recovered *a posteriori*. This major difference introduces a significant advantage, namely that as the laser focus is retained on top of the tracked particle, other spectroscopic parameters (e.g., fluorescence lifetime, emission spectrum, polarization, intensity dynamics) can be measured simultaneously with tracking of the particle [95]. For example, by measuring the fluorescence lifetime parallel to the tracking, the Förster resonance energy transfer (FRET)—and thus association events—can be precisely detected so as to provide information regarding the exact moment and position where the particle interacted with a given target labeled with a FRET acceptor fluorophore.

In a recent study, Hellriegel and Gratton [95] demonstrated the possibility of recording the fluorescence emission spectrum of different-colored fluorescent beads as they were followed in three dimensions using the orbiting-based method. This new capability was also applied to track small, fluorescently labeled protein assemblies in living cells.

This simultaneous multiparameter spectroscopy and 3-D tracking has opened a new window to exciting, new applications for SPT. In the future, tracking experiments will provide not only information with regards to the motion properties of the particle, but also information concerning the molecular parameters that may be used to construct a more complete view of dynamics in complex systems, such as the living cell.

Acknowledgments

These studies were supported in part by grants NIH-P41-RRO3155 and P50-GM076516 (to E.G.). V.L. is a member of CONICET, Argentina.

References

- 1 Weiss, S. (1999) Fluorescence spectroscopy of single biomolecules. *Science*, **283**, 1676–1683.
- 2 Axelrod, D., Koppel, D.E., Schlessinger, J., Elson, E., and Webb, W.W. (1976) Mobility measurement by analysis of fluorescence photobleaching recovery kinetics. *Biophys. J.*, **16**, 1055–1069.
- 3 Magde, D., Elson, E., and Webb, W.W. (1972) Thermodynamics fluctuations in a reactin system: measurement by fluorescence correlation spectroscopy. *Phys. Rev. Lett.*, **29**, 705–708.
- 4 Reits, E.A. and Neefjes, J.J. (2001) From fixed to FRAP: measuring protein mobility and activity in living cells. *Nat. Cell Biol.*, **3**, E145–E147.
- 5 Ruan, Q., Cheng, M.A., Levi, M., Gratton, E., and Mantulin, W.W. (2004) Spatial-temporal studies of membrane dynamics: scanning fluorescence correlation spectroscopy (SFCS). *Biophys. J.*, **87**, 1260–1267.
- 6 Digman, M.A., Brown, C.M., Sengupta, P., Wiseman, P.W., Horwitz, A.R., and Gratton, E. (2005) Measuring fast dynamics in solutions and cells with a laser scanning microscope. *Biophys. J.*, **89**, 1317–1327.
- 7 Hebert, B., Costantino, S., and Wiseman, P.W. (2005) Spatiotemporal image correlation spectroscopy (STICS) theory, verification, and application to protein velocity mapping in living CHO cells. *Biophys. J.*, **88**, 3601–3614.
- 8 Saxton, M.J. and Jacobson, K. (1997) Single-particle tracking: applications to membrane dynamics. *Annu. Rev. Biophys. Biomol. Struct.*, **26**, 373–399.
- 9 Saxton, M.J. (1994) Anomalous diffusion due to obstacles: a Monte Carlo study. *Biophys. J.*, **66**, 394–401.
- 10 Saxton, M.J. (1994) Single-particle tracking: models of directed transport. *Biophys. J.*, **67**, 2110–2119.
- 11 Saxton, M.J. (1997) Single-particle tracking: the distribution of diffusion coefficients. *Biophys. J.*, **72**, 1744–1753.
- 12 Saxton, M.J. (1996) Anomalous diffusion due to binding: a Monte Carlo study. *Biophys. J.*, **70**, 1250–1262.
- 13 Saxton, M.J. (1993) Lateral diffusion in an archipelago. Single-particle diffusion. *Biophys. J.*, **64**, 1766–1780.
- 14 Saxton, M.J. (1995) Single-particle tracking: effects of corrals. *Biophys. J.*, **69**, 389–398.
- 15 Qian, H., Sheetz, M.P., and Elson, E.L. (1991) Single particle tracking. Analysis of diffusion and flow in two-dimensional systems. *Biophys. J.*, **60**, 910–921.
- 16 Gelles, J., Schnapp, B.J., and Sheetz, M.P. (1988) Tracking kinesin-driven movements with nanometre-scale precision. *Nature*, **331**, 450–453.
- 17 Lee, G.M., Ishihara, A., and Jacobson, K. (1991) Direct observation of brownian motion of lipids in a membrane. *Proc. Natl Acad. Sci. USA*, **88**, 6274–6278.
- 18 Geerts, H., de Brabander, M., and Nuydens, R. (1991) Nanovid microscopy. *Nature*, **351**, 765–766.
- 19 Geerts, H., De Brabander, M., Nuydens, R., Geuens, S., Moeremans, M., De Mey, J., and Hollenbeck, P.J. (1987) Nanovid tracking: a new automatic method for the study of mobility in living cells based on colloidal gold and video microscopy. *Biophys. J.*, **52**, 775–782.
- 20 Levi, V. and Gratton, E. (2007) Exploring dynamics in living cells by tracking single particles. *Cell Biochem. Biophys.*, **48**, 1–15.
- 21 Carter, B., Shubeita, G., and Gross, S. (2005) Tracking single particles: a user-friendly quantitative evaluation. *Phys. Biol.*, **2**, 60–72.
- 22 Cheezum, M.K., Walker, W.F., and Guilford, W.H. (2001) Quantitative comparison of algorithms for tracking

- single fluorescent particles. *Biophys. J.*, **81**, 2378–2388.
- 23** Yildiz, A., Forkey, J.N., McKinney, S.A., Ha, T., Goldman, Y.E., and Selvin, P.R. (2003) Myosin V walks hand-over-hand: single fluorophore imaging with 1.5-nm localization. *Science*, **300**, 2061–2065.
- 24** Yildiz, A., Tomishige, M., Vale, R.D., and Selvin, P.R. (2004) Kinesin walks hand-over-hand. *Science*, **303**, 676–678.
- 25** Levi, V., Serpinskaya, A.S., Gratton, E., and Gelfand, V. (2006) Organelle transport along microtubules in *Xenopus* melanophores: evidence for cooperation between multiple motors. *Biophys. J.*, **90**, 318–327.
- 26** Fujiwara, T., Ritchie, K., Murakoshi, H., Jacobson, K., and Kusumi, A. (2002) Phospholipids undergo hop diffusion in compartmentalized cell membrane. *J. Cell Biol.*, **157**, 1071–1081.
- 27** Kusumi, A., Nakada, C., Ritchie, K., Murase, K., Suzuki, K., Murakoshi, H., Kasai, R.S., Kondo, J., and Fujiwara, T. (2005) Paradigm shift of the plasma membrane concept from the two-dimensional continuum fluid to the partitioned fluid: high-speed single-molecule tracking of membrane molecules. *Annu. Rev. Biophys. Biomol. Struct.*, **34**, 351–378.
- 28** Murase, K., Fujiwara, T., Umemura, Y., Suzuki, K., Iino, R., Yamashita, H., Saito, M., Murakoshi, H., Ritchie, K., and Kusumi, A. (2004) Ultrafine membrane compartments for molecular diffusion as revealed by single molecule techniques. *Biophys. J.*, **86**, 4075–4093.
- 29** Thompson, R.E., Larson, D.R., and Webb, W.W. (2002) Precise nanometer localization analysis for individual fluorescent probes. *Biophys. J.*, **82**, 2775–2783.
- 30** Sheppard, C.J.R. and Shotton, D.M. (1997) *Confocal Laser Scanning Microscopy*, Springer-Verlag New York Inc., New York.
- 31** Levi, V., Gelfand, V.I., Serpinskaya, A.S., and Gratton, E. (2006) Melanosomes transported by myosin-V in *Xenopus* melanophores perform slow 35 nm steps. *Biophys. J.*, **90**, L7–L9.
- 32** Spring, K.R. (2003) Cameras for digital microscopy, in *Digital Microscopy: A Second Edition of Video Microscopy*, vol. 72 (eds G. Sluder and D.E. Wolf), Elsevier Academic Press, Amsterdam, pp. 87–132.
- 33** Oshiro, M. and Moomaw, B. (2003) Cooled vs. intensified vs. electron bombardment CCD cameras—applications and relative advantages, in *Digital Microscopy: A Second Edition of Video Microscopy*, vol. 72 (eds G. Sluder and D.E. Wolf), Elsevier Academic Press, Amsterdam, pp. 133–156.
- 34** Berland, K.M., Jacobson, K.A., Frenche, T., and Rajfur, Z. (2003) Electronic cameras for low-light microscopy, in *Digital Microscopy: A Second Edition of Video Microscopy*, vol. 72 (eds G. Sluder and D.E. Wolf), Elsevier Academic Press, Amsterdam, pp. 103–132.
- 35** Kural, C., Serpinskaya, A.S., Chou, Y., Goldman, R.D., Gelfand, V.I., and Selvin, P.R. (2007) Tracking melanosomes inside a cell to study molecular motors and their interaction. *Proc. Natl Acad. Sci. USA*, **104**, 5378–5382.
- 36** Graf, R., Rietdorf, J., and Zimmermann, T. (2005) Live cell spinning disk microscopy. *Adv. Biochem. Eng. Biotechnol.*, **95**, 57–75.
- 37** Arhel, N., Genovesio, A., Kim, K.A., Miko, S., Perret, E., Olivo-Marin, J.C., Shorte, S., and Charneau, P. (2006) Quantitative four-dimensional tracking of cytoplasmic and nuclear HIV-1 complexes. *Nat. Methods*, **3**, 817–824.
- 38** Lange, S., Katayama, Y., Schmid, M., Burkacky, O., Brauchle, C., Lamb, D.C., and Jansen, R. (2008) Simultaneous transport of different localized mRNA species revealed by live-cell imaging. *Traffic*, **9**, 1256–1267.
- 39** Wazawa, T. and Ueda, M. (2005) Total internal reflection fluorescence microscopy in single molecule nanobiology. *Adv. Biochem. Eng. Biotechnol.*, **95**, 77–106.
- 40** Axelrod, D. (2001) Total internal reflection fluorescence microscopy in cell biology. *Traffic*, **2**, 764–774.
- 41** Sako, Y., Minoghchi, S., and Yanagida, T. (2000) Single-molecule imaging of EGFR signalling on the surface of living cells. *Nat. Cell Biol.*, **2**, 168–172.
- 42** Vale, R.D., Funatsu, T., Pierce, D.W., Romberg, L., Harada, Y., and Yanagida,

- T. (1996) Direct observation of single kinesin molecules moving along microtubules. *Nature*, **380**, 451–453.
- 43 Hell, S.W. (2007) Far-field optical nanoscopy. *Science*, **316**, 1153–1158.
- 44 Gustafsson, M.G. (2005) Nonlinear structured-illumination microscopy: wide-field fluorescence imaging with theoretically unlimited resolution. *Proc. Natl Acad. Sci. USA*, **102**, 13081–13086.
- 45 Rust, M.J., Bates, M., and Zhuang, X. (2006) Sub-diffraction-limit imaging by stochastic optical reconstruction microscopy (STORM). *Nat. Methods*, **3**, 793–795.
- 46 Betzig, E., Patterson, G.H., Sougrat, R., Lindwasser, O.W., Olenych, S., Bonifacino, J.S., Davidson, M.W., Lippincott-Schwartz, J., and Hess, H.F. (2006) Imaging intracellular fluorescent proteins at nanometer resolution. *Science*, **313**, 1642–1645.
- 47 Hess, S.T., Girirajan, T.P., and Mason, M.D. (2006) Ultra-high resolution imaging by fluorescence photoactivation localization microscopy. *Biophys. J.*, **91**, 4258–4272.
- 48 Sharonov, A. and Hochstrasser, R.M. (2006) Wide-field subdiffraction imaging by accumulated binding of diffusing probes. *Proc. Natl Acad. Sci. USA*, **103**, 18911–18916.
- 49 Egner, A., Geisler, C., von Middendorff, C., Bock, H., Wenzel, D., Medda, R., Andresen, M., Stiel, A.C., Jakobs, S., Eggeling, C., Schonle, A., and Hell, S.W. (2007) Fluorescence nanoscopy in whole cells by asynchronous localization of photoswitching emitters. *Biophys. J.*, **93**, 3285–3290.
- 50 Huang, B., Wang, W., Bates, M., and Zhuang, X. (2008) Three-dimensional super-resolution imaging by stochastic optical reconstruction microscopy. *Science*, **319**, 810–813.
- 51 Donnert, G., Keller, J., Medda, R., Andrei, M.A., Rizzoli, S.O., Luhrmann, R., Jahn, R., Eggeling, C., and Hell, S.W. (2006) Macromolecular-scale resolution in biological fluorescence microscopy. *Proc. Natl Acad. Sci. USA*, **103**, 11440–11445.
- 52 Sieber, J.J., Willig, K.I., Kutzner, C., Gerding-Reimers, C., Harke, B., Donnert, G., Rammner, B., Eggeling, C., Hell, S.W., Grubmüller, H., and Lang, T. (2007) Anatomy and dynamics of a supramolecular membrane protein cluster. *Science*, **317**, 1072–1076.
- 53 Kellner, R.R., Baier, C.J., Willig, K.I., Hell, S.W., and Barrantes, F.J. (2007) Nanoscale organization of nicotinic acetylcholine receptors revealed by stimulated emission depletion microscopy. *Neuroscience*, **144**, 135–143.
- 54 Kittel, R.J., Wichmann, C., Rasse, T.M., Fouquet, W., Schmidt, M., Schmid, A., Wagh, D.A., Pawlu, C., Kellner, R.R., Willig, K.I., Hell, S.W., Buchner, E., Heckmann, M., and Sigrist, S.J. (2006) Bruchpilot promotes active zone assembly, Ca²⁺ channel clustering, and vesicle release. *Science*, **312**, 1051–1054.
- 55 Westphal, V., Rizzoli, S.O., Lauterbach, M.A., Kamin, D., Jahn, R., and Hell, S.W. (2008) Video-rate far-field optical nanoscopy dissects synaptic vesicle movement. *Science*, **320**, 246–249.
- 56 Göppert-Mayer, M. (1931) Über Elementarakte mit zwei Quantensprüngen. *Ann. Phys.*, **9**, 273–295.
- 57 Denk, W., Strickler, J.H., and Webb, W.W. (1990) Two-photon laser scanning fluorescence microscopy. *Science*, **248**, 73–76.
- 58 Diaspro, A., Bianchini, P., Vicidomini, G., Faretta, M., Ramoino, P., and Usai, C. (2006) Multi-photon excitation microscopy. *Biomed. Eng. Online*, **5**, 36.
- 59 Diaspro, A., Chirico, G., and Collini, M. (2005) Two-photon fluorescence excitation and related techniques in biological microscopy. *Q. Rev. Biophys.*, **38**, 97–166.
- 60 So, P.T., Dong, C.Y., Masters, B.R., and Berland, K.M. (2000) Two-photon excitation fluorescence microscopy. *Annu. Rev. Biomed. Eng.*, **2**, 399–429.
- 61 Svoboda, K. and Yasuda, R. (2006) Principles of two-photon excitation microscopy and its applications to neuroscience. *Neuron*, **50**, 823–839.
- 62 Bornfleth, H., Edelmann, P., Zink, D., Cremer, T., and Cremer, C. (1999) Quantitative motion analysis of subchromosomal foci in living cells

- using four-dimensional microscopy. *Biophys. J.*, **77**, 2871–2886.
- 63** Speidel, M., Jonas, A., and Florin, E.L. (2003) Three-dimensional tracking of fluorescent nanoparticles with subnanometer precision by use of off-focus imaging. *Opt. Lett.*, **28**, 69–71.
- 64** Prabhat, P., Gan, Z., Chao, J., Ram, S., Vaccaro, C., Gibbons, S., Ober, R.J., and Ward, E.S. (2007) Elucidation of intracellular recycling pathways leading to exocytosis of the Fc receptor, FcRn, by using multifocal plane microscopy. *Proc. Natl Acad. Sci. USA*, **104**, 5889–5894.
- 65** Toprak, E., Balci, H., Blehm, B.H., and Selvin, P.R. (2007) Three-dimensional particle tracking via bifocal imaging. *Nanoletters*, **7**, 2043–2045.
- 66** Kao, H.P. and Verkman, A.S. (1994) Tracking of single fluorescent particles in three dimensions: use of cylindrical optics to encode particle position. *Biophys. J.*, **67**, 1291–1300.
- 67** Holtzer, L., Meckel, T., and Schmidt, T. (2007) Nanometric three-dimensional tracking of individual quantum dots in cells. *Appl. Phys. Lett.*, **90**, 053902, 1–3.
- 68** Saffarian, S. and Kirchhausen, T. (2008) Differential evanescence nanometry: live-cell fluorescence measurements with 10-nm axial resolution on the plasma membrane. *Biophys. J.*, **94**, 2333–2342.
- 69** Sarkar, A., Robertson, R.B., and Fernandez, J.M. (2004) Simultaneous atomic force microscope and fluorescence measurements of protein unfolding using a calibrated evanescent wave. *Proc. Natl. Acad. Sci. USA*, **101**, 12882–12886.
- 70** Kis-Petikova, K. and Gratton, E. (2004) Distance measurement by circular scanning of the excitation beam in the two-photon microscope. *Microsc. Res. Tech.*, **63**, 34–49.
- 71** Levi, V., Ruan, Q., and Gratton, E. (2005) 3-D particle tracking in a two-photon microscope: application to the study of molecular dynamics in cells. *Biophys. J.*, **88**, 2919–2928.
- 72** Levi, V., Ruan, Q., Plutz, M., Belmont, A.S., and Gratton, E. (2005) Chromatin dynamics in interphase cells revealed by tracking in a two-photon excitation microscope. *Biophys. J.*, **89**, 4275–4285.
- 73** Enderlein, J. (2000) Tracking of fluorescent molecules diffusing within membranes. *Appl. Phys. B*, **71**, 773–777.
- 74** Berland, K.M., So, P.T., and Gratton, E. (1995) Two-photon fluorescence correlation spectroscopy: method and application to the intracellular environment. *Biophys. J.*, **68**, 694–701.
- 75** Lessard, G., Goodwin, P.M., and Werner, J.H. (2007) Three-dimensional tracking of individual quantum dots. *Appl. Phys. Lett.*, **91**, 224106, 1–3, 6.
- 76** Vazquez, J., Belmont, A.S., and Sedat, J.W. (2001) Multiple regimes of constrained chromosome motion are regulated in the interphase *Drosophila* nucleus. *Curr. Biol.*, **11**, 1227–1239.
- 77** Heun, P., Laroche, T., Shimada, K., Furrer, P., and Gasser, S.M. (2001) Chromosome dynamics in the yeast interphase nucleus. *Science*, **294**, 2181–2186.
- 78** Heard, E. and Bickmore, W. (2007) The ins and outs of gene regulation and chromosome territory organisation. *Curr. Opin. Cell Biol.*, **19**, 311–316.
- 79** Lichter, P., Cremer, T., Borden, J., Manuelidis, L., and Ward, D.C. (1988) Delineation of individual human chromosomes in metaphase and interphase cells by in situ suppression hybridization using recombinant DNA libraries. *Hum. Genet.*, **80**, 224–234.
- 80** Cremer, T., Cremer, C., Schneider, T., Baumann, H., Hens, L., and Kirsch-Volders, M. (1982) Analysis of chromosome positions in the interphase nucleus of Chinese hamster cells by laser-UV-microirradiation experiments. *Hum. Genet.*, **62**, 201–209.
- 81** Branco, M.R. and Pombo, A. (2006) Intermingling of chromosome territories in interphase suggests role in translocations and transcription-dependent associations. *PLoS Biol.*, **4**, e138.
- 82** Cremer, T. and Cremer, C. (2006) Rise, fall and resurrection of chromosome territories: a historical perspective. Part I. The rise of chromosome territories. *Eur. J. Histochem.*, **50**, 161–176.
- 83** Branco, M.R. and Pombo, A. (2007) Chromosome organization: new facts,

- new models. *Trends Cell Biol.*, **17**, 127–134.
- 84** Kurz, A., Lampel, S., Nickolenko, J.E., Bradl, J., Benner, A., Zirbel, R.M., Cremer, T., and Lichter, P. (1996) Active and inactive genes localize preferentially in the periphery of chromosome territories. *J. Cell Biol.*, **135**, 1195–1205.
- 85** Chambeyron, S., Da Silva, N.R., Lawson, K.A., and Bickmore, W.A. (2005) Nuclear re-organisation of the Hoxb complex during mouse embryonic development. *Development*, **132**, 2215–2223.
- 86** Volpi, E.V., Chevret, E., Jones, T., Vatcheva, R., Williamson, J., Beck, S., Campbell, R.D., Goldsworthy, M., Powis, S.H., Ragoussis, J., Trowsdale, J., and Sheer, D. (2000) Large-scale chromatin organization of the major histocompatibility complex and other regions of human chromosome 6 and its response to interferon in interphase nuclei. *J. Cell Sci.*, **113** (Pt 9), 1565–1576.
- 87** Robinett, C.C., Straight, A., Li, G., Wilhelm, C., Sudlow, G., Murray, A., and Belmont, A.S. (1996) *In vivo* localization of DNA sequences and visualization of large-scale chromatin organization using lac operator/repressor recognition. *J. Cell Biol.*, **135**, 1685–1700.
- 88** Belmont, A.S., Li, G., Sudlow, G., and Robinett, C. (1999) Visualization of large-scale chromatin structure and dynamics using the lac operator/lac repressor reporter system. *Methods Cell Biol.*, **58**, 203–222.
- 89** Marshall, W.F., Straight, A., Marko, J.F., Swedlow, J., Dernburg, A., Belmont, A., Murray, A.W., Agard, D.A., and Sedat, J.W. (1997) Interphase chromosomes undergo constrained diffusional motion in living cells. *Curr. Biol.*, **7**, 930–939.
- 90** Chubb, J.R., Boyle, S., Perry, P., and Bickmore, W.A. (2002) Chromatin motion is constrained by association with nuclear compartments in human cells. *Curr. Biol.*, **12**, 439–445.
- 91** Rosa, A., Maddocks, J.H., Neumann, F.R., Gasser, S.M., and Stasiak, A. (2006) Measuring limits of telomere movement on nuclear envelope. *Biophys. J.*, **90**, L24–L26.
- 92** Tumber, T. and Belmont, A.S. (2001) Interphase movements of a DNA chromosome region modulated by VP16 transcriptional activator. *Nat. Cell Biol.*, **3**, 134–139.
- 93** Hediger, F., Taddei, A., Neumann, F.R., and Gasser, S.M. (2004) Methods for visualizing chromatin dynamics in living yeast. *Methods Enzymol.*, **375**, 345–365.
- 94** Chuang, C.H., Carpenter, A.E., Fuchsova, B., Johnson, T., de Lanerolle, P., and Belmont, A.S. (2006) Long-range directional movement of an interphase chromosome site. *Curr. Biol.*, **16**, 825–831.
- 95** Hellriegel, C. and Gratton, E. (2009) Real-time multi-parameter spectroscopy and localization in three-dimensional single-particle tracking. *J. R. Soc. Interface*, **6** (Suppl. 1), S3–S14.